Research article

Non-isothermal crystallization kinetics of graphene/PA10T composites

Xubing Fu [a], Xia Dong [b], Guisheng Yang [c,*], Shulin Bai [a,**]

[a] School of Materials Science and Engineering, HEDPS/Center for Applied Physics and Technology, Key Laboratory of Polymer Chemistry and Physics of Ministry of Education, Peking University, Beijing 100871, PR China
[b] Beijing National Laboratory for Molecular Science, CAS Key Laboratory of Engineering Plastics, Institute of Chemistry, Chinese Academy of Science, Beijing 100190, PR China
[c] Shanghai Genius Advanced Material Co., Ltd., Shanghai 201109, PR China

A R T I C L E   I N F O

A B S T R A C T

Crystallization kinetics is the key factor in controlling the polymer crystallization process and affecting crystallinity and crystalline morphology, which determine the polymer's main properties. In this work, the non-isothermal crystallization kinetics of graphene/PA10T composites are investigated by the Jeziorny method and Mo method, and the crystallization activation energy is calculated by the Kissinger method. It is found that the addition of an appropriate amount of graphene to PA10T can significantly promote the crystallization of PA10T and accelerate its crystallization rate. The Jeziorny equation does not have a linear relationship across the whole crystallization range, while the Mo equation does a good linear fitting. In addition, the crystallization activation energy decreases when the graphene content is below 1 wt.%. TGA results indicate that the addition of graphene improves the thermal stability of PA10T.

1. Introduction

Polymers can be divided into crystalline and amorphous categories according to the regularity of their molecular arrangement [1]. Polymer molecular chains with crystalline structures present a long-range ordered state. Crystallization is a process in which polymer segments transition from an amorphous to an ordered state, via nucleation and grain growth steps [2]. However, most crystalline polymers cannot be completely crystallized, and are referred to as semi-crystalline polymers. Semi-crystalline polymers are composed of crystalline and amorphous regions, and the proportion of the crystalline region relative to the overall polymer is referred to as crystallinity [3]. Because the boundaries between crystalline and the amorphous regions in polymers are often not very clear, measurement of crystallinity cannot be very accurate.

Crystallinity and crystalline morphology determine the main properties of crystalline polymers, and crystallization kinetics are the key control factor of the crystallization process. Therefore, studying the crystallization kinetics of polymers is of utmost importance. Polymer crystallization can proceed isothermally or non-isothermally [4]. Isothermal crystallization kinetics are often limited to a narrow temperature range, but in practice, the production process for crystalline polymers such as polyamide is dynamic and non-isothermal. Therefore,

non-isothermal crystallization kinetics are closer to the real-world processing and molding process of commercial polymers. The main methods for studying non-isothermal crystallization kinetics include the Jeziorny method [5], Mo method [6] and other methods. Previous reports have shown that the Mo method is more suitable than the other methods for describing the non-isothermal crystallization process of polyamides [7, 8, 9, 10, 11, 12, 13].

Poly (decamethylene terephthalamide) (PA10T) is a semi-aromatic polyamide, synthesized by the polycondensation of terephthalic acid and diaminodecane and is used in the aerospace, automotive and 5G communication industries [14]. As a semi-aromatic polyamide, PA10T has excellent mechanical properties, heat resistance, dimensional stability, chemical corrosion resistance, hydrolysis resistance and good processability, and its water absorption is very low compared with other semi-aromatic polyamides [15]. Because the monomer diaminodecane is produced from the renewable resource castor oil, PA10T is a sustainable polymer and is the only bio-based semi-aromatic polyamide commercially synthesized at present. However, because the melting point of PA10T is close to its thermal decomposition temperature, it easily decomposes during melt processing and injection molding. Therefore, PA10T is always modified for use in practical applications. Traditionally, PA10T is mainly modified by the inclusion of a high content of glass fiber

---

or other commonly used modified fillers [16, 17]. However, the addition of high-content of glass fiber or other filler content significantly affects the comprehensive performance of PA10T.

Graphene is kind of two-dimensional thin-film carbon material with a hexagonal honeycomb lattice composed of carbon atoms in an sp^2 hybrid orbital. It is a nanomaterial with many excellent properties, such as, high electrical conductivity [18, 19, 20, 21], thermal conductivity [22, 23, 24], and superconductivity [25, 26, 27, 28, 29]. Graphene is also one of the thinnest and lightest as well as strongest and hardest materials [30, 31, 32]. The modification of PA10T with graphene is expected to significantly improve the comprehensive (mechanical and functional) properties of PA10T and further expand its application in high-end fields.

The addition of graphene has been reported to affect the crystallization process of other crystalline polymers. Shehzad et al. [33] prepared graphene/high-density polyethylene (HDPE) composites by *in-situ* polymerization. It was found that graphene promotes the nucleation of HDPE by reducing the activation energy and increasing the crystallization initiation temperature. However, excessive graphene hinders the crystal growth rate. Bin-Dahman et al. [34] prepared starch/graphene/polyvinyl alcohol composites, finding that graphene promotes the crystallization of composites by reducing the effective activation energy. However, does not significantly change the crystallization half-time, indicating that the role of graphene is more prominent in the nucleation stage. Alvaredo et al. [35] studied the effect of graphene nanosheets (GNP) in the melt crystallization and cold crystallization of polyetheretherketone (PEEK) composites. Their results show that GNP has a nucleation effect, leading to the melt crystallizing at a higher temperature. In addition, GNP limits the fluidity of the polymer chains, extending the crystallization time. Graziano et al. [36] report the thermal stability, thermal deformation and crystallization behavior of a reduced graphene oxide (rGO) reinforced polyethylene/polypropylene dual-phase polyolefin system, confirming that rGO promotes the nucleation of crystals and improves the crystallization performance of polyethylene. The rare earth nucleating agent (WBG-II) is an additive for isotactic polypropylene copolymer (IPP), dissolving into the IPP melt during heating and reintegrating into different forms through self-assembly during cooling. He et al. [37] studied the effect of graphene oxide (GO) on the self-assembly of WBG-II. They showed that GO provided additional atomic nuclei for the self-assembly of WBG-II through hydrogen bond interactions and that GO and WBG-II had a synergistic effect on the crystallization of IPP. As can be seen, the role of graphene in promoting polymer crystallization and nucleation has been widely reported for many polymers; however, few studies have investigated the crystallization of graphene/semi-aromatic polyamide composites, let alone graphene/PA10T composites.

In this work, the effect of graphene on the non-isothermal crystallization of PA10T is examined. The graphene is used as a nucleation agent and the impact of graphene on crystallization morphology is investigated.

2. Materials and experimental procedure

2.1. Materials

Graphene powder (carbon content ≥99%) was provided by Ningbo Moxi Technology Co., Ltd., Ningbo, China. Purified terephthalic acid (PTA, 98%) was purchased from Sinopec Yangzi Petroleum Co., Ltd., Nanjing, China. Decanediamine (DA, 99%) was purchased from Wuxi Yinda Nylon Co., Ltd., Wuxi, China. H10 (heat stabilizer, 99%) was provided by Yuyao Hengze Chemical Co., Ltd., Ningbo, China. N$_2$ gas (99.9%) was provided by Hefei Zhongyi Chemical Products Co., Ltd., Hefei, China.

2.2. Preparation of graphene/PA10T composites

Graphene/PA10T composites were prepared by *in-situ* polymerization, and the preparation process is shown in Figure 1. Graphene was dispersed in deionized water by ultrasonic dispersion for 5–10 min. PTA (48.53 wt.%), DA (50.29 wt.%), H10 (1.18 wt.%) and graphene aqueous solutions were added into a reactor (high-temperature and high-pressure reaction kettle), and N$_2$ gas was added three times to maintain a certain pressure. The reactor was heated to 120 °C (holding pressure during heating), and this temperature was maintained for 1 h. The reactor was then heated to 300 °C (slow heating, holding pressure) and maintained at this temperature for 40 min. Next, the temperature of the reactor was increased to 320 °C, steam was released to release the pressure, and N$_2$ was used to purge the reactor. Stirring was stopped and the reactor contents were discharged, resulting in a graphene/PA10T composite. A sample of PA10T without graphene was prepared using the same procedure. PA10T and the graphene/PA10T composites were vacuum dried at 120 °C for 4 h. The final graphene/PA10T samples were denoted as PA10T-*x* (where *x* indicates the content of graphene, in *wt*.%).

3. Characterization

Raman spectroscopy measurements were undertaken using an HR Evolution laser Raman spectrometer (FRA, Horiba Jobin Yvon) with excitation provided in back-scattering geometry by a 532 nm argon laser line. Field-emission scanning electron microscopy (FE-SEM) images were obtained on a Hitachi S4800 field-emission SEM (JPN, Hitachi). Differential scanning calorimetry (DSC) was performed in nitrogen using a 6000 DSC analyzer (USA, PerkinElmer). The following test procedure was used: (1) 3 mg of sample was weighed and put into the crucible, which was placed in the DSC analyzer. (2) The sample was heated at rate of 20 °C/min from 50 to 350 °C and held at 350 °C for 5 min. (3) The temperature was reduced from 350 °C to 50 °C at a rate of 5 °C/min, 10 °C/min, 20 °C/min or 40 °C/min, and the DSC curve was recorded at
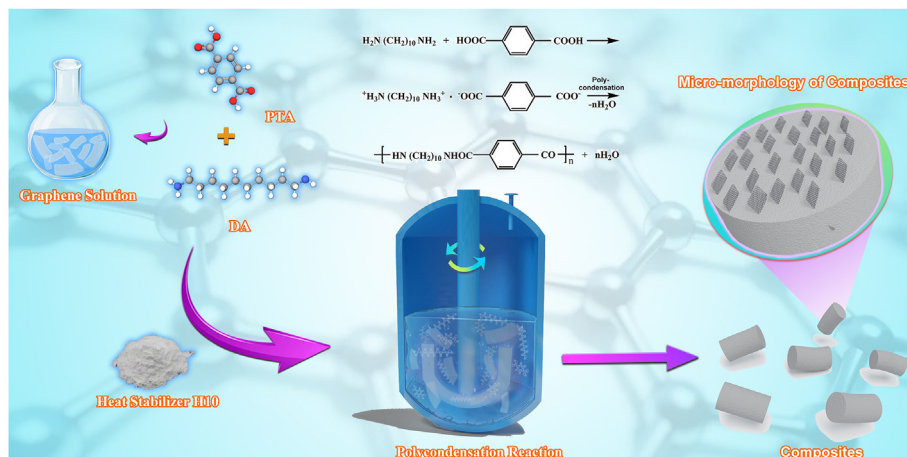
Figure 1. Schematic illustration for preparation process of graphene/PA10T composites.

constant temperature for 5 min. The microstructure of the nucleated crystals was observed by a Caikon XP-330 C (China, Caikon) polarized optical microscope (POM). The samples were heated from room temperature to 320 °C for 3 min, then cooled down to 270 °C for 60 min to observe the crystal morphology in thin films. Thermal gravimetric analysis (TGA) was performed using an SDT Q600 (USA, TA) at a heating rate of 20 °C/min from 50 to 700 °C in a nitrogen atmosphere.

4. Results and discussion

4.1. Structural and morphological characterization

As shown in Figure 2, graphene, PA10T and graphene/PA10T composites show characteristic peaks in the Raman spectrum scanning range of 1000–2800 cm^{-1}. The main characteristic peaks of graphene are the G peak at ~1580 cm^{-1} (related to the double degenerate phonon mode in the center of the Brillouin zone, reflecting the symmetry and crystallinity of graphene), the 2D peak at ~2710 cm^{-1} (originating from the second-order double resonance Raman scattering in the first Brillouin zone, reflecting the energy band structure of graphene) and the D peak at ~1350 cm^{-1} (originating from the phonon branch near the K point in the first Brillouin zone, requiring a defect activation). The D peak of the graphene powder is significantly less intense than the G and 2D peaks, an indication that the graphene has a low level of defects [38, 39]. The main peak of the Raman spectrum of the PA10T and graphene/PA10T samples is located at approximately 1636 cm^{-1}, corresponding to the vibration of the C=O double bond. This is the Raman characteristic peak of the amide I band. Another peak at 1550-1510 cm^{-1}, corresponding to the deformation vibration of the N–H bond, is the characteristic peak of the amide II band. The peak at 1440-1390 cm^{-1} corresponds to the stretching vibration of the C–N bond, and is the characteristic peak of the amide III band. The characteristic peaks at 1321, 1121 and 1066 cm^{-1} correspond to the vibrations of C–C, N–H and C–C bonds, respectively. Increasing the amount of graphene content in the graphene/PA10T composite increases the intensity of the graphene G and 2D peaks in the composite material Raman spectra.

SEM images of graphene and PA10T-1.0 composite are shown in Figure 3, the SEM image of pure PA10T is shown in Figure 4. Figure 3(a) and 3(b) show that the two-dimensional graphene film has a large sheet diameter as well as curls and wrinkles. The dispersion of graphene in the PA10T matrix, shown in Figure 3(c) and 3(d), is relatively uniform. In addition, the graphene sheets have a specific orientation, showing a trend of horizontal arrangement and a tilt to the lower right. The uniform

Figure 2. Raman spectra of graphene/PA10T composites prepared by *in situ* polymerization.

dispersion of graphene in the PA10T matrix lays a foundation for good properties of the composites.

4.2. Non-isothermal crystallization behavior

In general, when nanofillers are added to a matrix of crystalline polymers, they have two effects on crystallization. On one hand, nanofillers promote crystallization by acting as heterogeneous nucleation points. On the other hand, nanofillers act as impurities, hindering polymer crystallization [40]. The non-isothermal DSC crystallization curves of PA10T and graphene/PA10T composites are shown in Figure 5, and the relevant data are given in Table 1. With an increase in cooling rate, the crystallization onset temperature (T_o), crystallization peak temperature (T_p) and crystallization end temperature (T_e) of PA10T all show a downward trend and the shape of the crystallization peak becomes broader, indicating a wider temperature range of crystallization. Crystallization of polymers follows the theory of "nucleation first and then growth", that is, molecular chains overcome a barrier and form crystal nuclei through molecular thermal motion and then the molecular chains grow into crystals around the center of the crystal nuclei [41, 42]. During crystallization, relaxation time is required for the polymer molecular chains to arrange in a regular manner and form the lattice. With a slower cooling rate, the system has a high temperature and long maintenance time. The polymer molecular chains have a high degree of molecular thermal motion and a long relaxation time, allowing the formation of crystals with a relatively perfect degree of crystallization. Because of this, the crystalline temperature range is narrow. With a faster cooling rate, there is less time for relaxation and the crystallization process is hindered, requiring crystallization at a lower temperature. Therefore, T_o, T_p and T_e will gradually move to lower temperatures. When the cooling rate increases, the degree of supercooling increases, and the polymer melt viscosity increases; therefore, the molecular chain movement is limited. There is not sufficient time to make a perfect crystal, and the polymer will continue to crystallize until the temperature is too low. Therefore, the temperature range of crystallization becomes larger and the crystallization peak becomes broader [43].

Compared with pure PA10T, the non-isothermal crystallization curves of the graphene/PA10T composites at different cooling rates show the following characteristics: First, the non-isothermal crystallization curves of the composites are generally similar to those of PA10T, that is, with an increase in cooling rate, T_o, T_p and T_e move to lower temperatures, the crystallization temperature range becomes larger, and the crystallization peak shape becomes wider. Second, at the same cooling rate, the T_o and T_p of the graphene/PA10T composites are higher than that of pure PA10T, indicating that graphene plays a heterogeneous nucleation role and accelerates the crystallization of PA10T. In addition, Figure 5 and Table 1 show that at the same cooling rate, the T_o and T_p of the composites show a trend of increasing with an increase in graphene content. This indicates that the increase in graphene content can provide additional nucleation points and accelerate the deposition of molecular chains to promote nucleation.

The relative crystallinity ($X_{(T)}$) of polymers at temperature T can be calculated by the ratio of the area of the crystallization curve between the initial crystallization temperature T_o and temperature T to the area of the whole crystallization curve. The equation between $X_{(T)}$ and T is as follows [44, 45, 46, 47, 48, 49, 50, 51, 52]:

$$X_{(T)} = \frac{\int_{T_o}^{T} \left(\frac{dH}{dT}\right) dT}{\int_{T_o}^{T_e} \left(\frac{dH}{dT}\right) dT} \tag{1}$$

where T is the crystallization temperature at time t. The $X_{(T)}$ vs. T curves of PA10T and graphene/PA10T composites at different cooling rates show an inverse "s" shape, as shown in Figure 6. For a temperature T corresponding to the same $X_{(T)}$, with an increase in cooling rate, a trend of moving to lower temperatures can be seen. This is due to the
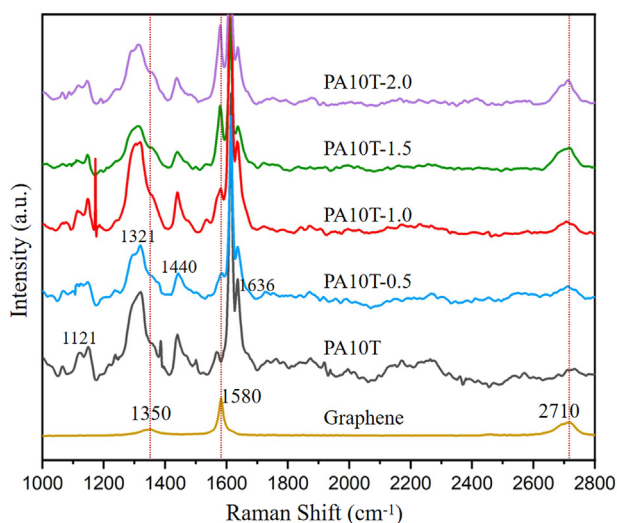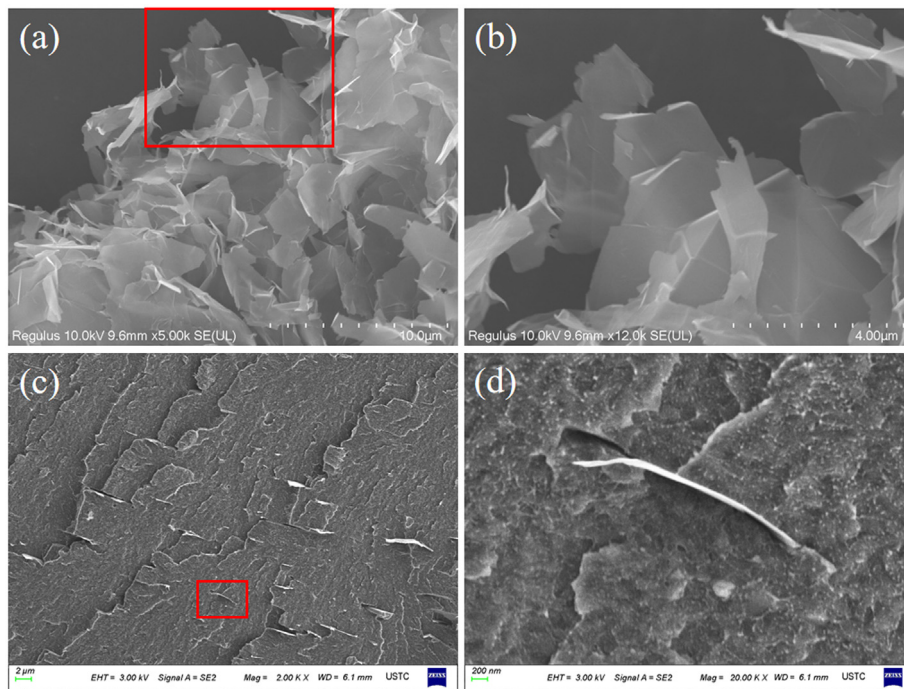
Figure 3. FE-SEM images of graphene and graphene/PA10T composites: (a) and (b) graphene, (b) magnified image of the red region in (a); (c) and (d) graphene/ PA10T composites, (d) magnified image of the red region in (c).
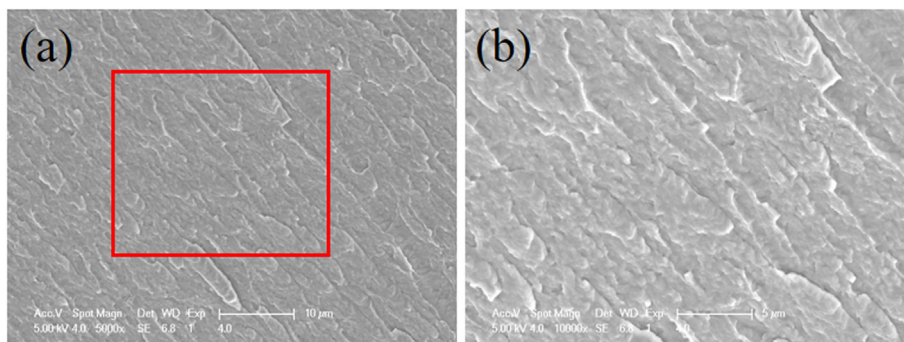
Figure 4. (a) The FE-SEM images of pristine PA10T, and (b) the magnified image of the red region in (a).

insufficient time for crystal nucleation and growth caused by the accelerated cooling rate. In addition, Figure 6 also shows that after the addition of graphene, the temperature T corresponding to the same $X_{(T)}$ for the graphene/PA10T composites is higher than that of pure PA10T, reflecting the heterogeneous nucleation properties of graphene.

Under non-isothermal conditions, crystallization time and temperature can be changed by modifying the cooling rate as follows [46, 47]:

$$t = \frac{T_o - T}{\varphi} \tag{2}$$

Where T is the crystallization temperature corresponding to time t, and Φ is the cooling rate. According to Eqs. (1) and (2), the relationship between relative crystallinity and time can be obtained, that is, the $X_{(t)}$ vs. t curve as shown in Figure 7. Figure 7 shows that the $X_{(t)}$ vs. t curves of PA10T and composites show "s" type curves under different cooling rates. For the same time t of $X_{(t)}$, an increasing cooling rate results in a shorter crystallization time. In addition, all curves are relatively flat at the early and late stages of crystallization. At the early stage of crystallization, this is because the temperature is high and molecular chains are rapidly moving, which is not conducive to the formation of crystal nuclei

and results in a slower crystallization rate. In the late stage of crystallization, molecular chain movement is limited due to the low temperature, and lower collision and extrusion between formed crystals lead to a decrease in the crystallization rate.

Table 1 shows the time when relative crystallinity is 50%, denoted $t_{1/2}$. At the same cooling rate, when the graphene content is 0.5–1.5 wt.%, the $t_{1/2}$ value of the composite is lower than that of pure PA10T and it shows a decreasing trend with an increase in graphene content. This is an indication that the presence of graphene accelerates the crystallization of PA10T, and when graphene content increases, the number of nucleation points also increases, accelerating the crystallization rate, and decreasing the crystallization time. With 2 wt.% graphene, the $t_{1/2}$ value of the composite is significantly higher than that of pure PA10T, indicating an increase in crystallization time. This is because when the content of graphene is too high, the viscosity of the system increases and molecular chain movement is hindered, delaying the crystallization rate and increasing the crystallization time. In addition, Table 1 also shows that for the same polymer, a faster cooling rate results in a shorter crystallization time, indicating that larger cooling rates are more conducive to the growth of crystal nuclei, which play a major role in the crystallization rate.
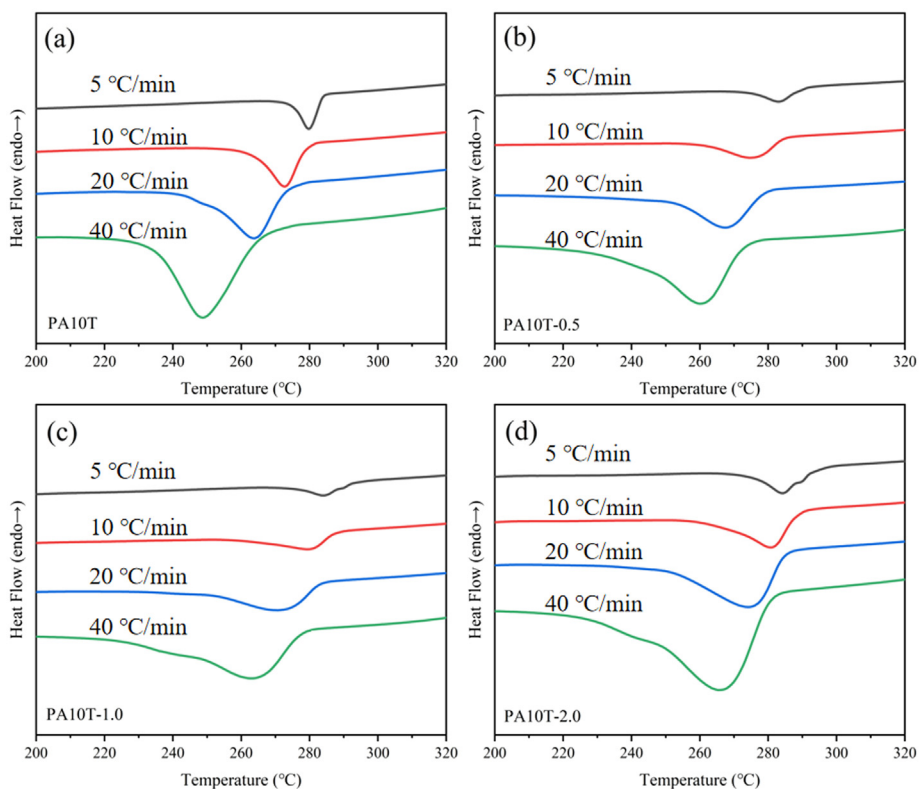
Figure 5. DSC curves of non-isothermal crystallization of PA10T and graphene/PA10T composites at different cooling rates: (a) pristine PA10T, (b) PA10T-0.5, (c) PA10T-1.0, and (d) PA10T-2.0.

Table 1. Non-isothermal crystallization parameters of PA10T and graphene/PA10T composites.

Samples	Φ (°C/min)	T_o (°C)	T_p (°C)	T_e (°C)	$t_{1/2}$ (min)
PA10T	5	283.9	279.3	274.9	1.5
	10	278.9	272.5	263.7	0.8
	20	273.2	264.0	249.0	0.5
	40	265.5	248.8	234.6	0.3
PA10T-0.5	5	289.6	284.2	275.3	1.4
	10	284.2	275.2	262.2	0.8
	20	278.6	268.0	253.4	0.5
	40	272.8	260.7	240.8	0.3
PA10T-1.0	5	290.0	284.4	277.1	1.4
	10	286.4	280.2	264.1	0.7
	20	282.0	270.7	254.9	0.5
	40	277.1	263.3	245. 1	0.3
PA10T-1.5	5	290.4	285.3	277.3	1.4
	10	286.7	280.7	269.3	0.7
	20	282.9	273.0	253.2	0.5
	40	277.3	264.1	240.8	0.3
PA10T-2.0	5	292.8	289.3	275.8	1.7
	10	288.3	281.1	265.7	1.0
	20	284.6	275.0	251.2	0.7
	40	280.5	266.0	240.9	0.4

4.3. Non-isothermal crystallization kinetics by Jeziorny method

The Avrami equation [48] (Eq. (3)) can be used to describe the isothermal crystallization kinetics of polymers, and Mandelkern [49] has claimed that it can also be used for the non-isothermal crystallization of polymers based on the assumption that the crystallization temperature is constant. The Mandelkern equation is obtained by transforming the Avrami equation into a different form (Eq. (4)). Based on the Mandelkern equation, Jeziorny et al. modified the rate constant in the isothermal crystallization process with the cooling rate (Eq. (5)) to eliminate the influence of the cooling rate, obtaining the Jeziorny equation [5], which describes the non-isothermal crystallization kinetics of polymers:

$$1 - x_{(t)} = \exp(-Z_t^{\,n}) \tag{3}$$

$$\lg\{-\ln[1 - x_{(t)}]\} = n\lg t + \lg Z_t \tag{4}$$

$$\lg Z_c = \frac{\lg Z_t}{\varphi} \tag{5}$$

where n is the Avrami index, Z_t is the kinetic rate constant during isothermal crystallization, and Z_c is the kinetic rate constant during non-isothermal crystallization. Using $\lg\{-\ln[1 - X_{(t)}]\}$ as the ordinate and $\lg t$ as the abscissa, the curve of $\lg\{-\ln[1 - X(t)]\}$ vs. $\lg t$ can be obtained, shown in Figure 8 for PA10T and the graphene/PA10T composites. Therefore, the values of Z_c and n can be obtained. Larger values of Z_c, represent faster crystallization rates. The Avrami index n is an important parameter reflecting the mechanism of nucleation and crystal growth in the polymer crystallization process. When the value of n is between 1 and 2, crystallization mainly occurs via one-dimensional fibrous growth. When it is between 2 and 3, crystallization mainly occurs via two-dimensional sheet growth. When it is between 3 and 4, crystallization mainly occurs via three-dimensional sphere growth. If the value of n is greater than 4, a complex multi-dimensional crystallization process exists. In practice, the growth mode of crystals is difficult to perfectly control along one morphology, and crystals tend to exist with a dominant morphology coexisting with other morphologies.

Figure 8 shows that the Jeziorny equation curve does not have a linear relationship cross the entire crystallization region. Using the
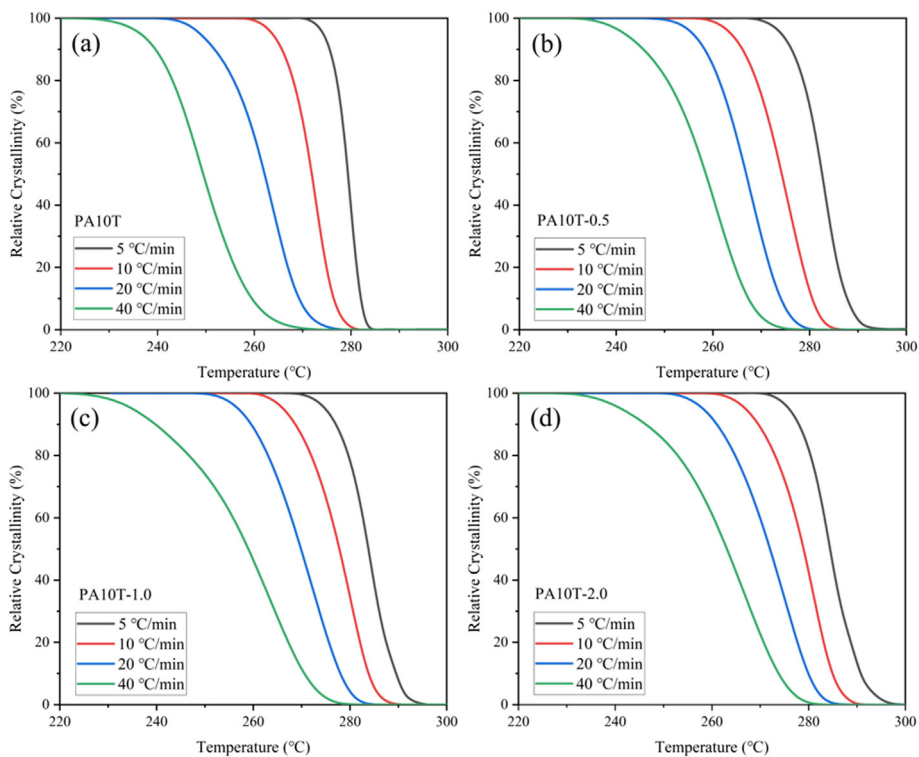
Figure 6. Relative crystallinity-temperature curves of PA10T and graphene/PA10T composites: (a) pristine PA10T, (b) PA10T-0.5, (c) PA10T-1.0, and (d) PA10T-2.0.
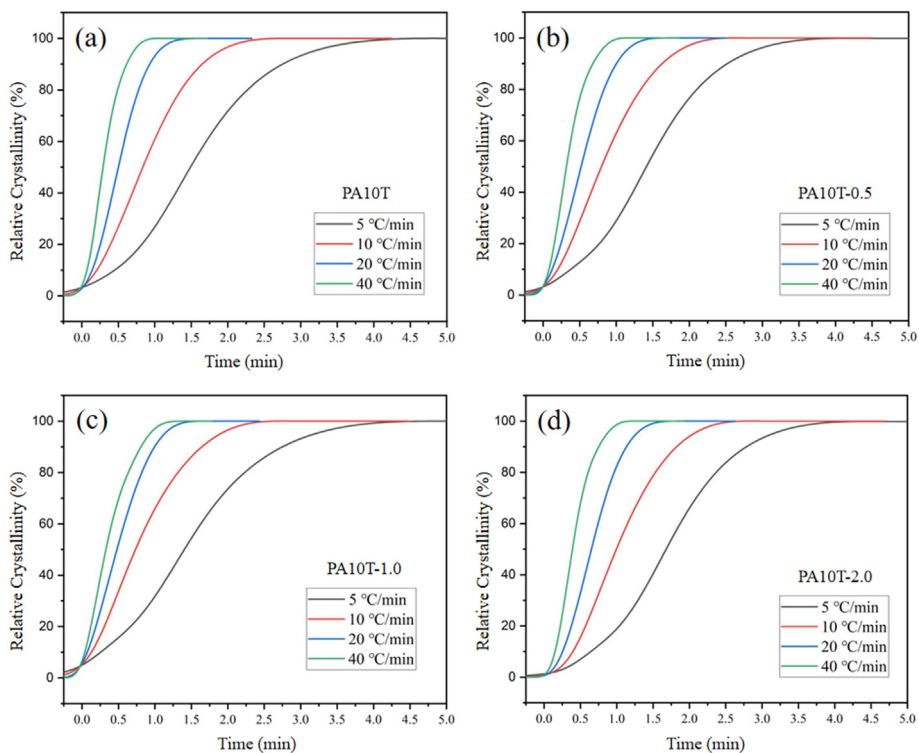
Figure 7. Relative crystallinity-time curves of PA10T and graphene/PA10T composites: (a) pristine PA10T, (b) PA10T-0.5, (c) PA10T-1.0, and (d) PA10T-2.0.

middle segment of the curve for linear fitting, relevant linear fitting parameters are shown in Table 2. As can be seen, the Z_c value of the majority of the samples increases with an increase in the cooling rate. At an equivalent cooling rate, the value of Z_c first increases and then decreases with increasing graphene loading in the graphene/PA10T composites.

This indicates that a low amount of graphene (<1.5 wt.%) promotes nucleation, improves the crystallization rate and increases the non-isothermal crystallization kinetic rate constant. However, when the graphene content is further increased (≥1.5 wt.%), the steric hindrance effect of graphene sheets on the polymer molecular chains is more
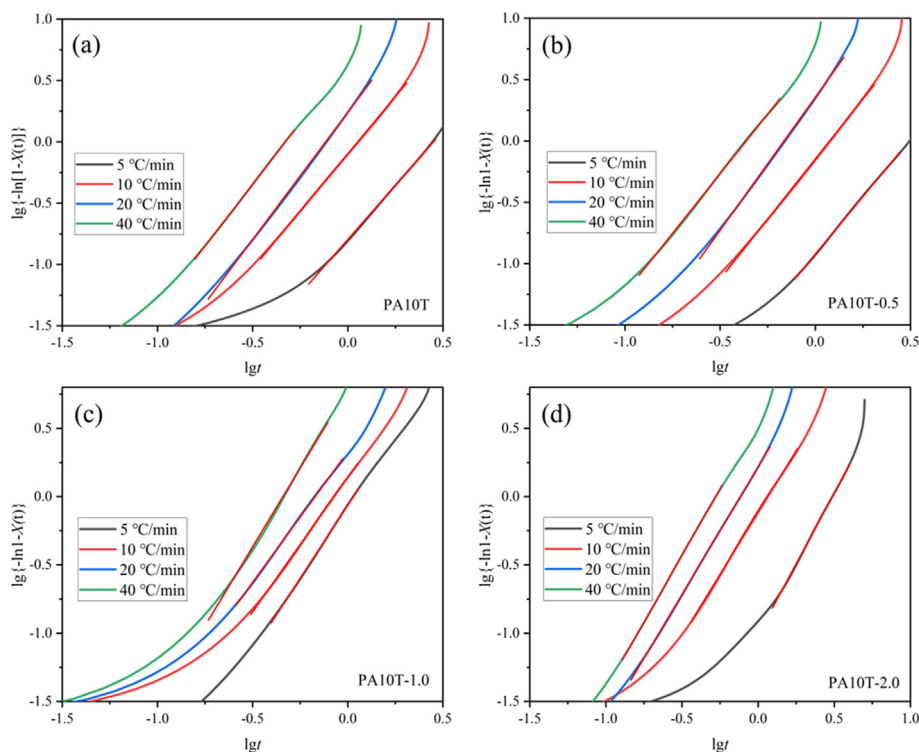
Figure 8. The lg{−ln[1 − X(t)]}—lgt curves of non-isothermal crystallization of PA10T and graphene/PA10T composites: (a) pristine PA10T, (b) PA10T-0.5, (c) PA10T-1.0, and (d) PA10T-2.0.

Table 2. Jeziorny parameters of non-isothermal crystallization kinetics for PA10T and graphene/PA10T composites.

Samples	Φ (°C/min)	n	Z_t	Z_c
PA10T	5	1.768	0.537	0.756
	10	1.869	0.799	0.978
	20	2.077	1.745	1.028
	40	2.012	4.577	1.039
PA10T-0.5	5	1.872	0.370	0.820
	10	1.956	0.712	0.997
	20	2.166	2.269	1.041
	40	1.946	5.080	1.041
PA10T-1.0	5	2.141	1.156	0.971
	10	1.967	0.720	1.033
	20	1.912	2.128	1.043
	40	2.310	6.118	1.046
PA10T-1.5	5	1.698	0.460	0.849
	10	1.753	0.844	0.983
	20	2.013	1.685	1.017
	40	1.791	2.679	1.026
PA10T-2.0	5	2.070	0.242	0.753
	10	1.811	0.764	0.973
	20	1.870	1.653	1.025
	40	1.952	3.512	1.032

pronounced, reducing the mobility of the molecular chain segments and also reducing the crystallization rate, resulting in a decrease in the value of Z_c. In addition, Table 2 shows that the n values corresponding to different cooling rates are also different, indicating that the cooling rate affects the crystallization morphology of the polymer. The n values of pristine PA10T are in the range of 1.768–2.012, which confirms the one-dimensional fibrous growth of PA10T. When the graphene content is 0.5–1.5 wt.%, the n values are obtained in the ranges of 1.872–2.166,

1.912–2.31, 1.698–2.013 and 1.811–2.07 respectively, suggesting one-dimensional fibrous and two-dimensional sheet growth. The polarized microscope (POM) images are illustrated in Figure 9. As shown in Figure 9, it is difficult to identify the typical spherulitic structure. Therefore, the theoretical kinetic models are supported by this experimental POM observation. Because the n value is not an integer, the nucleation process of PA10T and the graphene/PA10T composites have both homogeneous and heterogeneous nucleation processes.

4.4. Non-isothermal crystallization kinetics by the Mo method

The Avrami equation reflects the relationship between relative crystallinity $X_{(t)}$ and time t, and the Ozawa equation reflects the relationship between relative crystallinity $X_{(T)}$ and temperature T. Mo et al. [6] combined these two equations with Eq. (2) to obtain the following equation:

$$\lg\phi = \lg F(T) - \alpha \lg t \tag{6}$$

This formula is called the Mo equation (Eq. (6)), where $F(T)$ is the cooling rate required to reach a certain $X_{(T)}$ ($F(T)=(K_T/Z_t)^{1/m}$, K_T is the rate constant of the Ozawa equation), and $\alpha = n/m$ (n is the Avrami index and m is the Ozawa index). The Mo equation reflects the relationship between cooling rate, crystallization rate, temperature and time. It has been demonstrated that the Mo equation is more suitable for analyzing the entire non-isothermal crystallization process of polymers, especially the non-isothermal crystallization process of polyamide [7, 8, 9, 10, 11, 12, 13]. In contrast, the Jeziorny method is only applicable to part of the crystallization process, as described in the previous section. In the Mo equation, the relationship between lgΦ and lg$t$ is expressed as lg$\Phi = -\alpha$lg$t$ + lg$F(T)$. The relationship between lgΦ and lg$t$ is shown in Figure 10, where $-\alpha$ is the slope, and lg$F(T)$ is the y-intercept. As can be seen, a strong linear relationship is present for both pure PA10T and the graphene/PA10T composites. The values of α and $F(T)$ can be calculated from the fitting line data and are listed in Table 3. The value of $F(T)$ for all
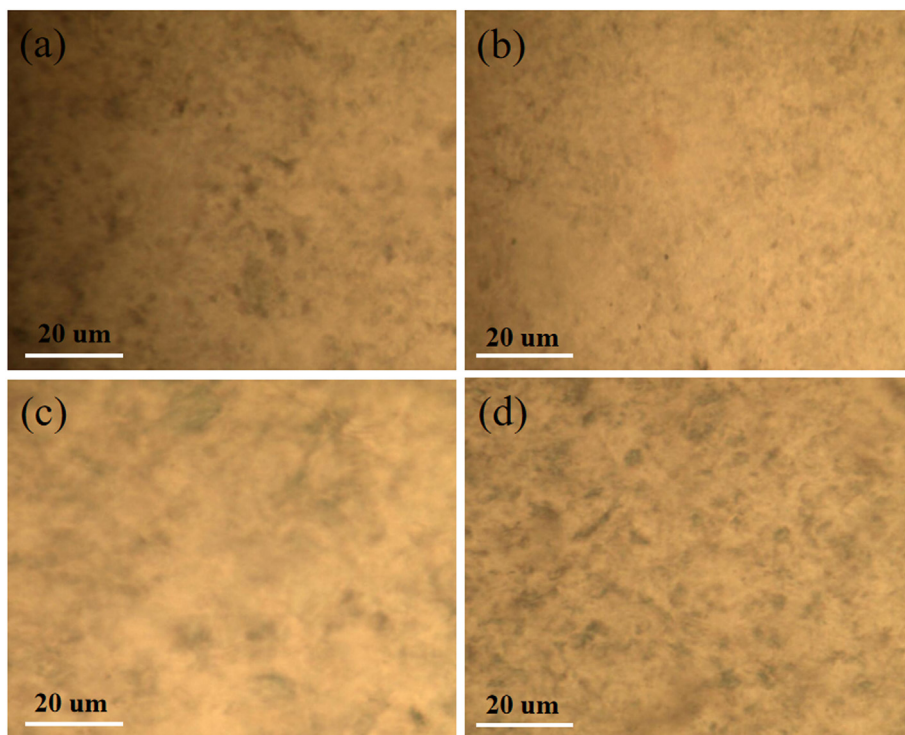
Figure 9. POM images of PA10T and graphene/PA10T composites: (a) pristine PA10T, (b) PA10T-0.5, (c) PA10T-1.0, and (d) PA10T-2.0.

samples increases with an increase in $X_{(t)}$, indicating that for a greater cooling rate, the value of $X_{(t)}$ also increases. With the addition of graphene up to 1.5 wt.%, the value of $F(T)$ of the graphene/PA10T composite is lower than that of pure PA10T, indicating that adding a low amount of graphene reduces the value of $F(T)$ and accelerates the crystallization rate. However, when the graphene content reaches 2 wt.%, the value of $F(T)$ increases and is higher than that of pure PA10T. Therefore, it can be concluded that too much graphene affects the crystallization of PA10T by hindering the movement of molecular chains, consistent with the discussion in Section 4.2.
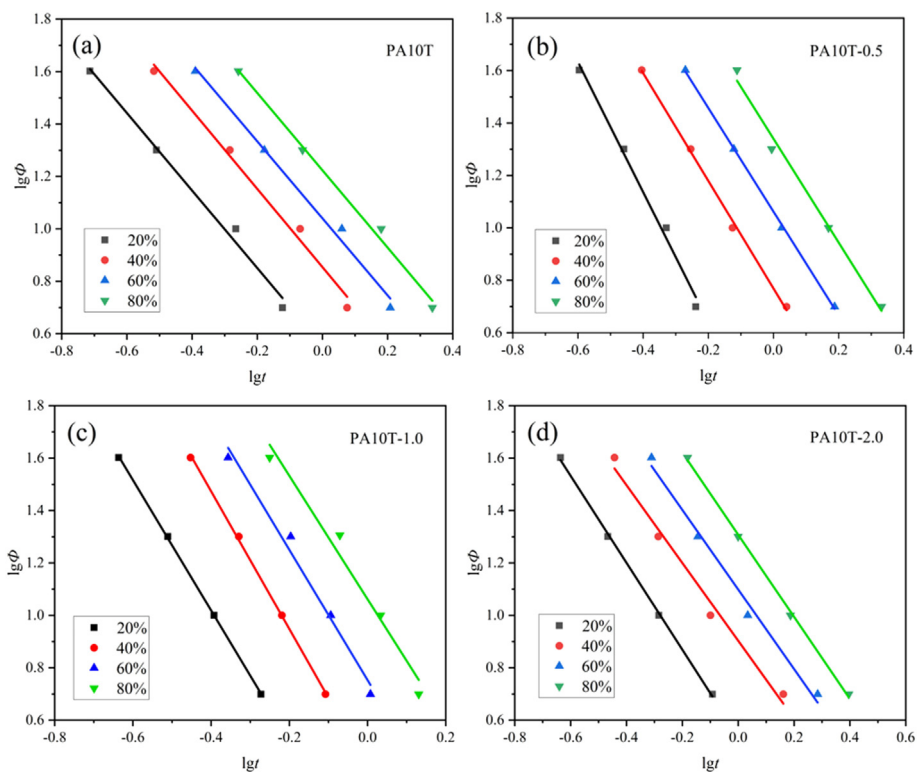
Figure 10. The lgΦ-lg$t$ curves of non-isothermal crystallization of PA10T and graphene/PA10T composites: (a) pristine PA10T, (b) PA10T-0.5, (c) PA10T-1.0, and (d) PA10T-2.0.

Table 3. Mo parameters of non-isothermal crystallization kinetics for PA10T and graphene/PA10T composites.

Samples	$X_{(t)}$ (%)	α	$F(T)$
PA10T	20	1.479	3.587
	40	1.493	7.146
	60	1.470	10.968
	80	1.476	16.737
PA10T-0.5	20	2.482	1.393
	40	2.054	5.872
	60	1.978	11.539
	80	1.981	21.891
PA10T-1.0	20	2.488	1.055
	40	2.627	2.646
	60	2.486	5.661
	80	2.354	11.527
PA10T-1.5	20	1.933	2.448
	40	1.854	5.760
	60	1.806	10.218
	80	1.808	17.438
PA10T-2.0	20	1.659	3.445
	40	1.485	7.998
	60	1.518	12.551
	80	1.567	20.303

Figure 11. The $\ln(\Phi/T_p^2)$-$1/T_p$ curves of non-isothermal crystallization of PA10T and graphene/PA10T composites.

Table 4. The non-isothermal crystallization activation energy of PA10T and graphene/PA10T composites.

Samples	PA10T	PA10T-0.5	PA10T-1.0	PA10T-1.5	PA10T-2.0
ΔE (KJ/mol)	−258.502	−236.820	−226.295	−239.865	−259.010

4.5. Crystallization activation energy

The crystallization process of crystalline polymers is generally controlled by two factors. One is the free energy barrier of crystal nucleation and the other is the activation energy of crystal unit transport across the phase boundary. The activation energy is related to the energy and potential barrier, which is an important parameter in the process of phase transition. It represents the energy required to overcome the potential barrier in polymer crystallization, and is therefore an important indicator in judging the crystallization ability of a polymer. The methods for calculating crystallization activation energy include the Kissinger method [50], Friedman method [51, 52], Takhor method [53] and Vyazovkin method [54, 55, 56]. The Kissinger method is the most commonly used method and its equation is as follows (Eq. (7)):

$$\frac{d\left[\ln\left(\phi/T_p{}^2\right)\right]}{d\left(1/T_p\right)} = -\frac{\Delta E}{R} \tag{7}$$

where Φ is the cooling rate, T_p is the crystallization peak temperature, and ΔE is the activation energy of non-isothermal crystallization and R is the gas constant (8.314 J/(mol·K)). A graph can be plotted with $\ln(\Phi/T_p^2)$ as the ordinate and $1/T_p$ as the abscissa, shown in Figure 11 for PA10T and the graphene/PA10T composites. A good linear fit was obtained for all materials. The slope-$\Delta E/R$ data of the fitting linear fit can be obtained from the graph, and the non-isothermal crystallization activation of PA10T and the graphene/PA10T composites is calculated as shown in Table 4. The absolute value of ΔE first decreases and then increases with an increase in graphene content, indicating that a low amount of graphene ($\leq$1.5 wt.%) can act as a nucleating agent to promote crystallization, manifested as the decrease in crystallization activation energy. When the content of graphene continues to increase ($>$1.5 wt.%), the graphene sheets can hinder the movement of molecular chains, shown by the increase in crystallization activation energy [57]. This is not conducive to crystallization. These results are consistent with the trends in graphene wt.% seen in the calculation for crystallization time, kinetic rate constant Z_c (Jeziorny method) and cooling rate $F(T)$ (Mo method).
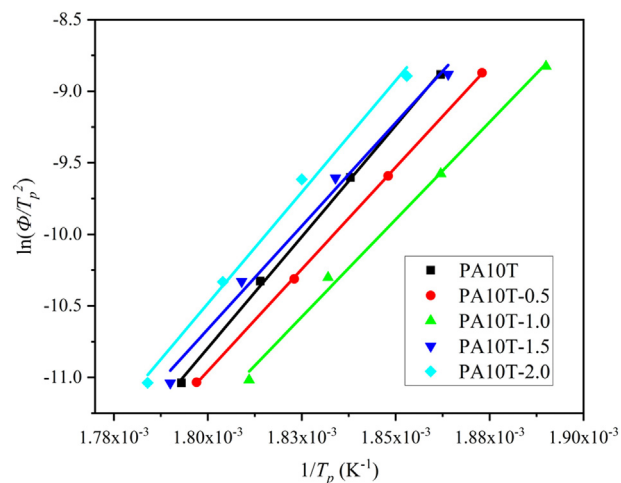
4.6. Thermal stability

The thermal stability of PA10T and graphene/PA10T composites is an important property for their potential use as high-performance engineering plastics. TGA is used to study the degradation and thermal stability of polymer composites [58]. TGA curves of PA10T and the graphene/PA10T composites are shown in Figure 12, and the relevant data are listed in Table 5. Figure 12 shows that in the range of 200–700 °C under a nitrogen atmosphere, the thermal degradation process of PA10T is a one-step decomposition process of random chain breaking. This conforms to the thermal degradation mechanism of the general polycondensation reaction. For PA10T and the graphene/PA10T composites, the 5 wt.% weight loss below 430 °C is mainly due to the decomposition of unpolymerized monomers and oligomers. The main weight loss in the temperature range of 430–520 °C is the decomposition of high molecular weight polymers. In addition, the mass loss at each temperature point in the range of 490–520 °C tends to decrease with increasing graphene content. Moreover, the temperature at which 5
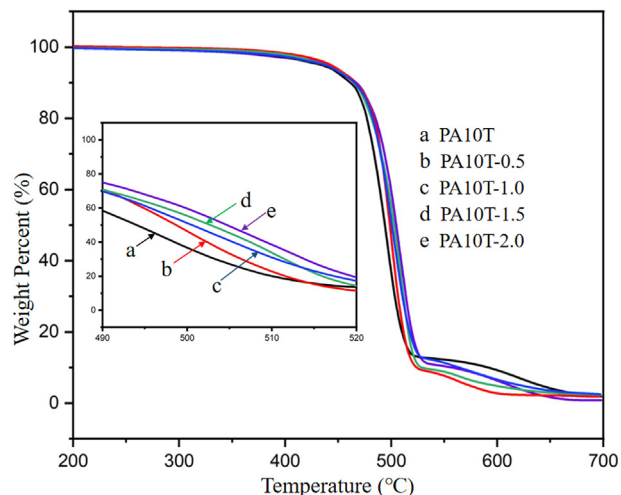
Figure 12. The TGA curves of pristine PA10T and graphene/PA10T composites.

Table 5. TGA data of PA10T and graphene/PA10T composites.

Samples	$T_{5\ wt.\%}$ (°C)	$T_{10\ wt.\%}$ (°C)	$T_{50\ wt.\%}$ (°C)	Residue at 680 °C (*wt.%*)
PA10T	433.97	461.24	493.97	2.38
PA10T-0.5	442.55	465.73	498.53	2.34
PA10T-1.0	437.37	465.66	500.26	2.68
PA10T-1.5	437.87	464.47	502.53	2.59
PA10T-2.0	439.71	466.82	504.42	2.18

wt.%, 10 wt.% and 50 wt.% of the composites is lost increases with increasing graphene content, which shows that the addition of graphene can improve the thermal stability of PA10T. The 50 wt.% weight loss temperatures (T$_{50\ wt.\%}$) increased by 4.56–10.45 °C, as shown in Table 5. However, the improvement is not easy to distinguish due to the low graphene content.

5. Conclusions

In this work, the non-isothermal crystallization kinetics of PA10T and graphene/PA10T composites are studied. First, the non-isothermal crystallization behavior shows that the addition of graphene to PA10T increases the crystallization temperature, and the addition of graphene (0.5–1.5 wt.%) accelerates the crystallization rate of PA10T. Second, the non-isothermal crystallization kinetics of PA10T and graphene/PA10T composites show that the Jeziorny equation does not have a linear relationship across the whole crystallization range, while the Mo equation does have a good linear fitting. Third, the Kissinger equation was used to study the non-isothermal crystallization activation energy. When the graphene content in the graphene/PA10T composites is below 1.5 wt.%, the heterogeneous nucleation effect promoting the crystallization of PA10T is significant. When the graphene content is up to 1.5 wt.%, the movement of molecular chains is obstructed, hindering crystallization of PA10T. With an increase in graphene content from 0.5 to 2.0 wt.%, the crystallization activation energy of the graphene/PA10T composites shows a trend of first decreasing and then increasing. In this study, 1.0 wt.% graphene was determined to be the ideal level of graphene content for enhancing the rate of crystallization and reducing the crystallization activation energy for graphene/PA10T composites.

The crystallization behavior of polymers significantly influences mechanical properties, so the study of crystallization kinetics of PA10T and graphene/PA10T composites is critical for the further investigation of its mechanical, electrical and thermal properties. The addition of an appropriate amount of graphene to promote the crystallization of PA10T is expected to improve the strength of PA10T and enhance functional properties such as thermal and electrical conductivity, providing a polymer composite with more suitable properties than pure PA10T for applications in the aerospace, automotive and communication industries.

Declarations

Author contribution statement

Xubing Fu: Conceived and designed the experiments; Performed the experiments; Analyzed and interpreted the data; Contributed reagents, materials, analysis tools or data; Wrote the paper.

Xia Dong: Conceived and designed the experiments.

Guisheng Yang: Conceived and designed the experiments; Contributed reagents, materials, analysis tools or data.

Shulin Bai: Conceived and designed the experiments; Analyzed and interpreted the data.

Declaration of interests

The authors declare no conflict of interest.

References

[1] W.B. Chen, P. Chen, G. Zhang, G.L. Xing, Y. Feng, Y.W. Yang, et al., Macrocycle-derived hierarchical porous organic polymers: synthesis and applications, Chem. Soc. Rev. 50 (20) (2021) 11684–11714.

[2] N.E. Persson, P.H. Chu, M. McBride, M. Grover, E. Reichmanis, Nucleation, growth, and alignment of poly(3-hexylthiophene) nanofibers for high-performance OFETs, Accounts Chem. Res. 50 (4) (2017) 932–942.

[3] S. Rastogi, D.R. Lippits, G.W.M. Peters, R. Graf, Y.F. Yao, H.W. Spiess, Heterogeneity in polymer melts from melting of polymer crystals, Nat. Mater. 4 (8) (2005) 635–641.

[4] N. Zirak, M. Shirinbayan, S. Farzaneh, A. Tcharkhtchi, Effect of molecular weight on crystallization behavior of poly (lactic acid) under isotherm and non-isotherm conditions, Polym. Adv. Technol. 33 (4) (2022) 1307–1316.

[5] A. Jeziorny, Parameters characterizing the kinetics of the non-isothermal crystallization of poly (ethylene terephthalate) determined by DSC, Polymer 19 (10) (1978) 1142–1144.

[6] T.X. Liu, Z.S. Mo, Non-isothermal melt and cold crystallization kinetics of poly (aryl ether ether ketone ketone), Polym. Eng. Sci. 37 (3) (1997) 568–573.

[7] Y.L. Ma, G.S. Hu, X.L. Ren, B.B. Wang, Non-isothermal crystallization kinetics and melting behaviors of nylon 11/tetrapod-shaped ZnO whisker (T-ZnOW) composites, Mat. Sci. Eng. A: Struct. 460 (2007) 611–618.

[8] G.Y. Xu, Y.L. Zhuang, R. Xia, J.Y. Cheng, Y.C. Zhang, Carbon nanotubes induced nonisothermal crystallization of ultrahigh molecular weight polyethylene with reduced chain entanglements, Mater. Lett. 89 (2012) 272–275.

[9] Y. Liu, G.S. Yang, Non-isothermal crystallization kinetics of polyamide-6/graphite oxide nanocomposites, Thermochim. Acta 500 (1) (2010) 13–20.

[10] J.S. Shi, X.J. Yang, X. Wang, L.D. Lu, Non-isothermal crystallization kinetics of nylon 6/attapulgite nanocomposites, Polym. Test. 29 (5) (2010) 596–602.

[11] M.Y. Liu, Q.X. Zhao, Y. Wang, C.G. Zhang, Z.S. Mo, S.K. Cao, Melting behaviors, isothermal and non-isothermal crystallization kinetics of nylon 1212, Polymer 44 (8) (2003) 2537–2545.

[12] Q.X. Zhang, Z.S. Mo, Melting crystallization behavior of nylon 66, Chin. J. Polym. Sci. 19 (3) (2001) 237–246.

[13] Q.X. Zhang, Z.H. Zhang, H.F. Zhang, Z.S. Mo, Isothermal and nonisothermal crystallization kinetics of nylon-46, J. Polym. Sci., Polym. Phys. Ed. 40 (16) (2002) 1784–1793.

[14] X. Tong, Z. Wang, M.L. Zhang, X.J. Wang, G. Zhang, S.R. Long, et al., Synthesis, characterization and non-isothermal crystallization kinetics of a new family of poly(ether-block-amide)s based on nylon 10T/10I, Polymers 13 (1) (2021) 72, 1-22.

[15] T.H. Ai, W.T. Feng, G.J. Zou, Z.L. Ren, P.L. Wang, J.H. Ji, et al., High-performances biobased semi-aromatic polyamide 10T copolymerized with silicone monomers, J. Appl. Polym. Sci. 138 (16) (2021), e50266.

[16] J.B. Guo, J. Wang, Y.F. Wu, Y. He, H.S. Song, X.L. Chen, Thermal stability and thermal degradation kinetics of short and long glass fiber reinforced PA10T composites, Polym. Eng. Sci. 59 (2) (2019) 246–253.

[17] J. Wang, Y. He, L.M. Jin, D.F. Zhou, J.B. Guo, Influence of thermo-oxidative aging on the dynamical mechanical properties and thermal degradation kinetics of glass fiber-reinforced PA10T composites, Polym. Eng. Sci. 59 (3) (2019) 643–656.

[18] N.A.H. Castro, F. Guina, N.M.R. Peters, K.S. Novoselov, A.K. Geim, The electronic properties of graphene, Rev. Mod. Phys. 81 (1) (2009) 109–162.

[19] X. Du, I. Skachko, A. Barker, E.Y. Andrei, Approaching ballistic transport in suspended graphene, Nat. Nanotechnol. 3 (8) (2008) 491–495.

[20] Y.B. Zhang, Y.W. Tan, H.L. Stormer, P. Kim, Experimental observation of the quantum hall effect and berry's phase in graphene, Nature 438 (7065) (2005) 201–204.

[21] K.I. Bolotin, K.J. Sikes, Z. Jiang, M. Klima, G. Fudenberg, J. Hone, et al., Ultrahigh electron mobility in suspended graphene, Solid State Commun. 146 (9-10) (2008) 351–355.

[22] J.H. Seol, I. Jo, A.L. Moore, L. Lindsay, Z.H. Aitken, M.T. Pettes, et al., Two-dimensional phonon transport in supported graphene, Science 328 (5975) (2010) 213–216.

[23] A.A. Balandin, S. Ghosh, W.Z. Bao, I. Calizo, D. Teweldebrhan, F. Miao, et al., Superior thermal conductivity of single-layer graphene, Nano Lett. 8 (3) (2008) 902–907.

[24] H. Malekpour, A.A. Balandin, Raman-based technique for measuring thermal conductivity of graphene and related materials, J. Raman Spectrosc. 49 (1) (2018) 106–120.

[25] Y. Cao, V. Fatemi, A. Demir, S. Fang, S.L. Tomarken, J.Y. Luo, et al., Correlated insulator behaviour at half-filling in magic-angle graphene superlattices, Nature 556 (7699) (2018) 80–84.

[26] Y. Cao, V. Fatemi, S. Fang, K. Watanabe, T. Taniguchi, E. Kaxiras, et al., Unconventional superconductivity in magic-angle graphene superlattices, Nature 556 (7699) (2018) 43–50.

[27] Y.W. Son, M.L. Cohen, S.G. Louie, Half-metallic graphene nanoribbons, Nature 444 (7117) (2006) 347–349.

[28] O. Hold, V. Barone, J.E. Peralta, G.E. Scuseria, Enhanced half-metallicity in edge-oxidized zigzag graphene nanoribbons, Nano Lett. 7 (8) (2007) 2295–2299.

[29] F. Schedin, A.K. Geim, S.V. Morozov, E.W. Hill, P. Blake, M.I. Katsnelson, et al., Detection of individual gas molecules adsorbed on graphene, Nat. Mater. 6 (9) (2007) 652–655.

[30] C. Lee, X. Wei, J.W. Kysar, J. Hone, Measurement of the elastic properties and intrinsic strength of monolayer graphene, Science 321 (5887) (2008) 385–388.

[31] R. Grantab, V.B. Shenoy, R.S. Ruoff, Anomalous strength characteristics of tilt grain boundaries in graphene, Science 330 (6006) (2010) 946–948.

[32] G.H. Lee, R.C. Cooper, S.J. An, S. Lee, A. Van der zande, N. Petrone, et al., High-strength chemical-vapor deposited graphene and grain boundaries, Science 340 (6136) (2013) 1073–1076.

[33] F. Shehzad, S.P. Thomas, M.A. Al-Harthi, Non-isothermal crystallization kinetics of high density polyethyene/graphene nanocomposites prepared by *in-situ* polymerization, Thermochim. Acta 589 (2014) 226–234.

[34] O.A. Bin-Dahman, F. Shehazd, M.A. Al-Harthi, Influence of graphene on the non-isothermal crystallization kinetics of poly (vinyl alcohol)/starch composite, J. Polym. Res. 25 (1) (2018) 1–10.

[35] A. Alvaredo, M.I. Martin, P. Castell, R.G.D. Villoria, J.P. Fernandez-Blazquez, Non-isothermal crystallization behavior of PEEK/graphene nanoplatelets composites from melt and glass states, Polymers 11 (1) (2019) 124.

[36] A. Graziano, O.A.T. Dias, C. Garcia, S. Jaffer, J. Tjong, M. Sain, Non-isothermal crystallization behavior and thermal properties of polyethylene tuned by polypropylene and reinforced with reduced graphene oxide, Nanomaterials 10 (8) (2020) 1428.

[37] M. He, H.H. Shi, B.B. Chang, G.Q. Zheng, W. Cao, C.T. Liu, C.Y. Shen, The synergistic effect of rare-earth complex nucleating agent and graphene oxide on the non-isothermal crystallization behavior of ipp originating from the diverse self-assembly morphology, Macromol. Chem. Phys. 222 (3) (2021) 2000357.

[38] F. Tuinstra, J.L. Koenig, Raman spectrum of graphite, J. Chem. Phys. 53 (3) (1970) 1126–1130.

[39] C. Thomsen, S. Reich, Double resonant Raman scattering in graphite, Phys. Rev. Lett. 85 (24) (2001) 5214–5217.

[40] M. Sattari, A. Molazemhosseini, M.R. Naimi-Jamal, A. Khavandi, Nonisothermal crystallization behavior and mechanical properties of PEEK/SCF/nano-SiO₂ composites, Mater. Chem. Phys. 147 (3) (2014) 942–953.

[41] Q.C. Fan, F.H. Duan, H.B. Guo, T. Wu, Non-isothermal crystallization kinetics of polypropylene and hyperbranched polyester blends, Chin. J. Chem. Eng. 23 (2) (2015) 441–445.

[42] A. Layachi, D. Frihi, H. Satha, R. Seguela, S. Gherib, Non-isothermal crystallization kinetics of polyamide 66/glass fibers/carbon black composites, J. Therm. Anal. Calorim. 124 (3) (2016) 1319–1329.

[43] Y. Wang, H.L. Kang, R. Wang, R.G. Liu, X.M. Hao, Crystallization of polyamide 56/polyamide 66 blends: non-isothermal crystallization kinetics, J. Appl. Polym. Sci. 135 (26) (2018), 46409.

[44] G. Maglio, E. Martuscelli, R. Palumbo, I. Soldati, Influence of intra-chain trans double bonds on the melt crystallization of polyamides, Polymer 17 (3) (1976) 185–191.

[45] J.T. Wan, Z.Y. Bu, C. Li, H. Fan, B.G. Li, Preparation, melting, glass relaxation and nonisothermal crystallization kinetics of a novel dendritic nylon-11, Thermochim. Acta 524 (2011) 117–127.

[46] S.P. Jape, V.D. Deshpande, Nonisothermal crystallization kinetics of nylon 66/LCP blends, Thermochim. Acta 655 (2017) 1–12.

[47] N.L.A. Mcferran, C.G. Armstrong, T. Mcnally, Nonisothermal and isothermal crystallization kinetics of nylon-12, J. Appl. Polym. Sci. 110 (2) (2010) 1043–1058.

[48] M. Avrami, Kinetics of phase change I. General theory, J. Chem. Phys. 7 (12) (1939) 1103–1113.

[49] L. Mandelkern, Crystallization of Polymers, Mc Graw-Hill Press, New York, 1964.

[50] H.E. Kissinger, Variation of peak temperature with heating rate in differential thermal analysis, J. Res. Natl. Bur. Stand. (U.S.) 57 (4) (1956) 217–221.

[51] H.L. Friedman, Thermal degradation of plastics. 1. The kinetics of polymer chain degradation, J. Polym. Sci. 45 (145) (1960) 119–125.

[52] H.L. Friedman, Kinetics of thermal degradation of char-forming plastics from thermogravimetry. Application to phenolic plastic, J. Polym. Sci. C: Polym. Sym. 6 (1964) 183.

[53] R. Takhor, Advances in Nucleation and Crystallization of Glasses, American Ceramics Society, Columbus, 1971, p. 166.

[54] S. Vyazovkin, Evaluation of activation energy of thermally stimulated solid-state reactions under arbitrary variation of temperature, J. Comput. Chem. 18 (3) (1997) 393–402.

[55] S. Vyazovkin, C.A. Wight, Model-free and model-fitting approaches to kinetic analysis of isothermal and nonisothermal data, Thermochim. Acta 341 (1999) 53–68.

[56] S. Vyazovkin, Modification of the integral isoconversional method to account for variation in the activation energy, J. Comput. Chem. 22 (2) (2001) 178–183.

[57] X. Xia, C. Xie, S. Cai, Non-isothermal crystallization behavior of low-density polyethylene/copper nanocomposites, Thermochim. Acta 427 (1) (2005) 129–135.

[58] J. Wang, L.T. Li, Y. He, H.S. Song, X.L. Chen, J.B. Gu, The effect of thermo-oxidative ageing on crystallization, dynamic and static mechanical properties of long glass fibre-reinforced polyamide 10T composites, R. Soc. Open Sci. 5 (6) (2018), 172029.